



HAL
open science

Dynamics of Forced Alternate Gravel Bars Under Unsteady Flow: an Experimental Investigation

Shashank Gupta, Céline Berni, Benoit Camenen

► **To cite this version:**

Shashank Gupta, Céline Berni, Benoit Camenen. Dynamics of Forced Alternate Gravel Bars Under Unsteady Flow: an Experimental Investigation. Proceedings of the 39th IAHR World Congress, 2022. hal-03948232

HAL Id: hal-03948232

<https://hal.inrae.fr/hal-03948232>

Submitted on 20 Jan 2023

HAL is a multi-disciplinary open access archive for the deposit and dissemination of scientific research documents, whether they are published or not. The documents may come from teaching and research institutions in France or abroad, or from public or private research centers.

L'archive ouverte pluridisciplinaire **HAL**, est destinée au dépôt et à la diffusion de documents scientifiques de niveau recherche, publiés ou non, émanant des établissements d'enseignement et de recherche français ou étrangers, des laboratoires publics ou privés.

Dynamics of Forced Alternate Gravel Bars Under Unsteady Flow: an Experimental Investigation

Shashank Gupta⁽¹⁾, Céline Berni⁽²⁾ and Benoit Camenen⁽³⁾

^(1,2,3) INRAE, UR RiverLy, Lyon-Villeurbanne, France
shashank.gupta@inrae.fr, celine.berni@inrae.fr, benoit.camenen@inrae.fr

Abstract

We investigated in this study the dynamics of forced alternate gravel bars under unsteady flow by laboratory experiments. We developed a reference case of two forced alternate gravel bars with the water worked methodology in an 18 m-long and 0.7 m-wide inclined flume. Forced alternate bars were formed through sequential transport, erosion, and sedimentation cycles, which is a way to reproduce the surface and subsurface properties of gravel-bed rivers. The first unsteady flow experiment was performed over the reference case with a constant sediment supply rate maintained throughout the experiment. The second unsteady flow experiment was performed without sediment supply over the bed topography obtained at the end of the first unsteady flow experiment to test the sediment input's impact. In both unsteady flow experiments, the first forced gravel bar became flatter and shorter, and the second forced bar disappeared when the water discharge approached its peak. The two forced alternate gravel bars redeveloped during the falling limb of the hydrograph with different shapes.

Keywords: Forced alternate bars; unsteady flow; gravel bar morphodynamics

1. INTRODUCTION

Alternate bars are large-scale bed-forms, generally observed in embanked straight rivers having half-width to water depth ratios greater than or equal to 6. They are characterized by large deposits of sediments on the alternate side of the river banks. They are broadly classified into two categories as free or forced alternate bars. Free alternate bars are formed due to an inherent instability originating between the flow-bed system and are migrating in nature. In contrast, forced alternate bars are formed due to a persistent forcing source across the river channel like bridge piers or distortion in the channel geometry like river bend. Forced alternate bars are non-migrating in nature, and their wavelengths are longer than free alternate bars. Such alternate bars may create various problems like reducing channel navigability, trapping fine sediments, inducing side bank erosion, increasing flood risk, etc. Predicting the geometrical features of alternate bars and understanding the change in those features due to discharge variability in the rivers are crucial for river managers and engineers to timely handle the problems they create.

Ikeda (1984) first proposed empirical relations to predict the wavelength and height of free alternate bars using laboratory data of several researchers. Theoretical investigations using linear stability analysis and weakly non-linear analysis, such as Colombini et al. (1987), resulted in the computation of free alternate bars wavelength, celerity, and bar height. They demonstrated a critical half-width to water depth ratio, below which no bars can be formed. Struiskma and Crosato (1989) theoretical model focused on the computation of wavelength of forced alternate bars. The model of Colombini et al. (1987) can also be used to evaluate the wavelength of the forced alternate bars at a linear scale. Some differences can be noticed in the predicted values of the wavelength of the forced alternate bars from the two models due to different underlying assumptions.

Tubino (1991) theoretical model was the first model to investigate the development of the amplitude of free alternate bars under unsteady flow conditions. He demonstrated that the free alternate bars response depends on the ratio between the time scale of the bar growth and the time scale of the unsteady flow/ flood event. The flow unsteadiness will control the final average bar amplitude if the two mentioned time scales are of the same order. He proposed a procedure to determine the final amplitude of the free alternate bars for a given flood event. A recent numerical study performed by Roline (2021) to study the development of forced alternate bars in varying discharge conditions around resonant conditions highlighted the presence of hysteresis in the behavior of forced alternate bars during the rising and falling limbs of a flood event. The wavelength of the forced alternate bars was long after the end of a flood event compared to the initial configuration. However, the observed behavior in the numerical simulations has yet to be validated by experiments.

In the present study, we will compare the wavelengths of observed forced alternate bars with the linear theory of Lanzoni (2000) and contribute to a better understanding of the behavior of forced alternate bars under

unsteady flow conditions through laboratory experiments. First, we developed a reference state of two forced alternate gravel bars in an 18-m long and 0.7-m wide tilting flume with an average bed slope of 0.063%. Then, two types of experiments were performed by launching a flood event with and without upstream sediment supply. The first unsteady experiment was launched on the reference state, and the second unsteady experiment was launched on the bed topography obtained at the end of the first unsteady experiment.

2. FLUME EXPERIMENT

The experiments were carried out in the tilting flume of the Hydraulic and Hydromorphology laboratory of INRAE, Lyon-Villeurbanne. The flume is 18 meters long and 1 meter wide and has sidewalls made of glass. A sketch of the flume is shown in Figure 1. The slope of the flume can be adjusted from 0 to 5 % and was set to 0.063 % for the experiments. The flume is equipped with a water recirculation system and a sediment supply system installed at the upstream end of the flume. The sediment supply system is a sediment reservoir set on a conveyor belt, and the drop point of the sediments in the flume is at $x = 0.83$ m (Figure 1). The working length of the flume is 17 meters, and the width of the flume was reduced to 0.7 meters by placing plastic plates in the flume for the present study. Experiments were handled with very well sorted gravels of median diameter $d_{50} = 3.5$ mm.

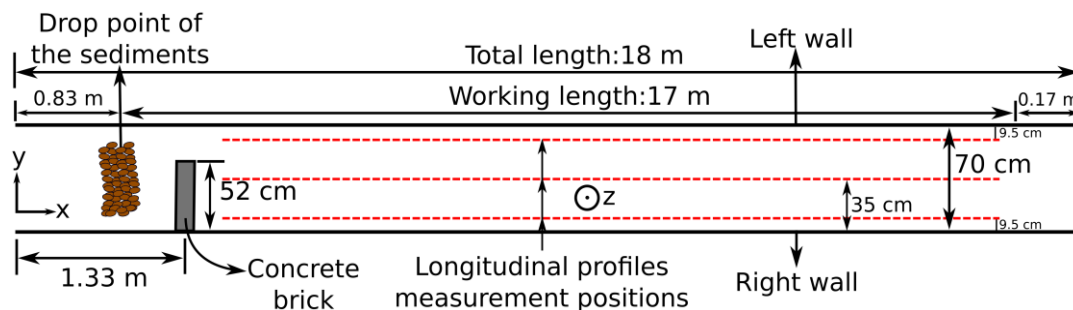


Figure 1. Sketch of the experimental flume with concrete block used to force the system persistently.

2.1 Data collection

The initial and final bed topographies were scanned using a laser scanner (MICRO-EPSILON scanControl 2900-100) in the transverse direction without water flow. The transverse profiles were measured at a resolution of 0.1 millimeters every 6 cm from $x = 2$ m to $x = 16.8$ m. While the experiment was running, water depths and bed elevations were measured using a combination of an Ultrasonic (Baumer UNDK 2016903/S35A) and a laser sensor (MICRO-EPSILON optoNCDT ILD-1220-100) every 60 cm from $x = 2$ m to $x = 17$ m. Three longitudinal profiles of water depths and bed elevations were measured, one along the centerline of the flume, and the other two were 9.5 cm from the right and left walls of the flume, respectively. The cross-section area and velocity of the sediment pile on the conveyor were used to estimate and control the instantaneous sediment input rate during the experiment. The sediments transported during an experimental run were collected by placing a metallic box at the downstream end of the flume. The averaged sediment transport rate was then calculated by dividing the dry weight of the sediments by the time of an experimental run.

2.2 Experimental protocol to develop the reference case (REF)

We set 70 cm-wide and 1 m-long gravel stabilizers (vertical honeycombs) on the flume floor before filling them with gravels. Then, a six cm-thick layer of gravel was laid out on top of it and screeded manually to make an initial erodible flatbed. The height of the downstream weir was set to the initial thickness of the bed to prevent the downstream erosion of the bed. A fine mesh horizontal honeycomb was placed at the beginning of the flume ($x = 0$ m) to strait the flow turbulence. A concrete block of 52 cm-width was placed at $x = 1.33$ m to force the system persistently. The initial slope of the flume was set to 0.0063. The water discharge was constant, $Q_w = 14.9 \pm 0.2$ l/s throughout the experiment. The conveyor supplied sediment at a predetermined constant rate of 14.6 ± 0.5 g/s. The sediment transport capacity of the water discharge, $Q_w = 14.9$ l/s at a bed slope of 0.0063, was nearly zero for a flatbed.

The sediment-feeding rate was set significantly larger than the sediment transport capacity of the flow in the channel in order to allow the bar formation through sequential cycles of deposits and transports. The experiment was paused when the downstream sediment collection metallic box was completely filled with sediments. Three intermediate stops were made during the experiment. The experiment was stopped when the final equilibrium conditions were reached, i.e., (a) measured sediment transport rate became equal to the sediment input rate, (b) the final bed slope became almost constant, and (c) the bar lengths became

approximately constant. Table 1 summarizes the experimental conditions of the three experiments conducted for the present study.

2.3 Experimental protocol for the unsteady flow experiments

The first unsteady flow experiment (UF1) was performed over the reference state of forced alternate bars with a constant sediment supply rate maintained throughout the experiment, which corresponds to the event-averaged expected sediment rate based on a previously established sediment rating curve. The second unsteady flow experiment (UF2) was performed without sediment supply over the bed topography obtained at the end of the first unsteady flow experiment to test the sediment input's impact. In both experiments, water input discharge followed a triangular-shaped symmetrical hydrograph, as shown in Figure 2. The minimum and peak discharge of the hydrograph was 10 l/s and 25 l/s, and the duration of the hydrograph was 5 hours. The constant input sediment supply rate of experiment UF1, $Q_{s,UF1}$ was calculated using the following expression:

$$Q_{s,UF1} = \frac{\int_0^T Q_s dt}{T} \quad [1]$$

where Q_s is the sediment transport capacity of the flow, and T is the duration of the experiment. Figure 2 shows the time series of the water discharge (Q_w) and corresponding sediment transport capacity (Q_s) of the flow for the triangular-shaped hydrograph, the constant water discharge used in the reference experiment ($Q_{w,REF}$) and the different constant sediment supply rates maintained during the three experiments.

Table 1. Summary of the experimental conditions

| Case | Duration: T [h] | Discharge: Q_w [l/s] | Sediment input rate: Q_s [g/s] | Initial Bed Slope: S_i [-] | Final Bed Slope: S_f [-] |
|------|----------------------|---------------------------|-------------------------------------|---------------------------------|-------------------------------|
| REF | 28 | 14.9 ± 0.2 | 14.6 ± 0.5 | 0.0063 | 0.0090 |
| UF1 | 5 | 10-25 | 21.1 ± 0.6 | 0.0090 | 0.0091 |
| UF2 | 5 | 10-25 | 0 | 0.0091 | 0.0057 |

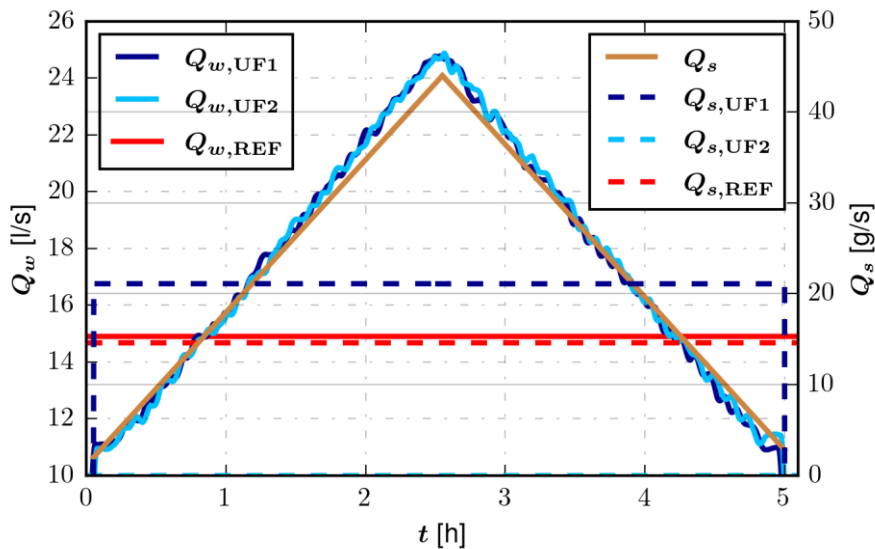


Figure 2. Time series of the water discharge (solid lines), sediment transport capacity corresponding to the hydrograph (in brown), and the constant coarse sediment supply rate (dashed lines) used for the different experiments. The sediment-rating curve is plotted for a 0.009 value of bed slope.

2.4 Methodology to compute the bar properties

Forced alternate bars are steady and have a zero migration rate, so they are mainly characterized by their wavelength and height. To compute the different bar properties of forced alternate bars, identification of individual bar units are required. We used the bed elevation data collected after the experiment to identify the bar units and compute the different metrics of forced alternate bars. We used a rectangular patch of four different widths ($0.1B$, $0.15B$, $0.2B$, and $0.25B$) to select the bed elevations symmetrically from the right and left sides of

the flume. Then for each selected patch of bed elevations, the bed elevations from the right and left sides were averaged in the transverse direction to have the right and left longitudinal profiles of bed elevations. Then, we took the difference between the left and right longitudinal profiles and computed the positions of the zero crossings. The wavelength of the forced alternate bars (λ_b) was defined as the distance between the n and $n + 2$ zero crossings. The length of the first and second forced bars was defined as the distance between the n and $n + 1$ zero crossings and $n + 1$ and $n + 2$ zero crossings. The elevation map of a bar unit was obtained by splitting the bed elevations data at the n and $n + 2$ zero crossings. The bed elevation data of a bar unit is then detrended by subtracting a fitted planar trend in the streamwise direction to compute the bar height and relief. The bar height (H_b) was computed by taking the difference between the highest and lowest detrended elevations within a bar unit (Ikeda, 1983). However, the bar height is sensitive to outliers and measurement errors. Therefore, the relief of the bars rather than the bar height could be more appropriate to characterize how high a bar is (Redolfi et al., 2020). The bar relief (R_b) is calculated by computing the standard deviation of all the detrended bed elevations within a bar unit. We computed the above-defined bar properties for each rectangular patch of four different widths and then averaged them to obtain a single value for an experiment.

To follow the evolution of the length of the alternate bars during the unsteady flow experiments, we used the left, and right longitudinal profiles of bed elevations measured 9.5 cm from the respective walls by the laser sensors. The height of the individual bars was difficult to measure using two longitudinal profiles of bed elevations during the experiment. So, we defined a proxy height of the alternate bars to see the evolution of the height of the bars qualitatively. We took the difference between the left and right longitudinal profiles and computed the positions of the zero crossings. The length of the bars was defined the same way as mentioned above. The proxy height of the alternate bars was determined using the difference profile of left and right bed elevations. The proxy height of the first and second forced bar was defined as the amplitudes of the crest and trough in the difference profile, respectively. We also computed the damping coefficient (ζ_b) of the forced alternate bars using their proxy heights as:

$$\zeta_b = 1 - \frac{H_2^P}{H_1^P} \quad [2]$$

where H_1^P and H_2^P are the proxy height of the first and second forced alternate bars.

2.5 Application of the linear theory of Lanzoni (2000)

We used the theory of Lanzoni (2000) to compute the linear solution of the two-dimensional shallow-water and Exner equations for a straight channel with constant width and downstream gradient. The linear solution gives the wavelength and damping coefficient of the forced alternate bars. Specifically, we used the following bedload transport formula, which is suited to our inclined flume:

$$\Phi = 5.87(\theta - \theta_{cr})^{1.5} \quad [3]$$

where Φ is the non-dimensional sediment transport rate per unit width, θ is the Shields number, and θ_{cr} is the critical Shields number, which is equal to 0.0468. In addition, the effect of the lateral bed slope on the direction of the bedload transport formula is modeled based on the bed leveling experiments of Talmon et al. (1995) as:

$$\tan(\beta) = - \frac{r}{\sqrt{\theta}} \frac{d\eta}{dy} \quad [4]$$

where β is the angle between the velocity vector and the sediment transport vector, and r is an empirical dimensional parameter typically ranging from 0.3 to 0.6. We used $r = 0.6$; a similar value was used in the forced bar model of Struiksmas and Crosato (1989). Struiksmas and Crosato (1989) demonstrated that the secondary flow effects did not play an essential role in developing forced alternate bars. Therefore, we neglected the secondary flow effects from the complete model of Lanzoni (2000). For simplicity, we also neglected the dispersive effects arising in the momentum equations due to performing the depth-averaging process. Furthermore, we assumed an initial flatbed and used the Keulegan (1938) logarithmic friction formula, which gives the following expression for the dimensionless Chézy coefficient:

$$c = 6 + 2.5 \log\left(\frac{D}{2.5 d_{50}}\right) \quad [5]$$

where D is the normal flow water depth, and d_{50} is the mean sediment size.

3. EXPERIMENTAL RESULTS

3.1 Reference case of forced alternate gravel bars

The reference case of forced alternate bars was developed by supplying sediments at a rate larger than the sediment transport capacity of the flow. As the experiment started, two processes took place simultaneously in the flume. The first process was that the slope of the bed began to increase due to the deposition of sediments in the upstream part of the flume to balance the sediment transport rate of the supply rate of the sediments. The second process was the formation of the forced alternate bars due to the curvature of streamlines near the concrete block. The first forced bar started to develop by successive deposition of the sediments in the left side of the first half of the flume. Once this first forced bar was high enough to force the downstream flow-bed system, the second bar started to develop. A system of two forced alternate gravel bars was developed at the end of the experiment, as shown in Figure 3. The forced bars reached their equilibrium features after eleven hours of the experiment. The equilibrium values of the wavelength and height of the forced alternate gravel bars were 12.5 m and 9.6 cm, respectively.

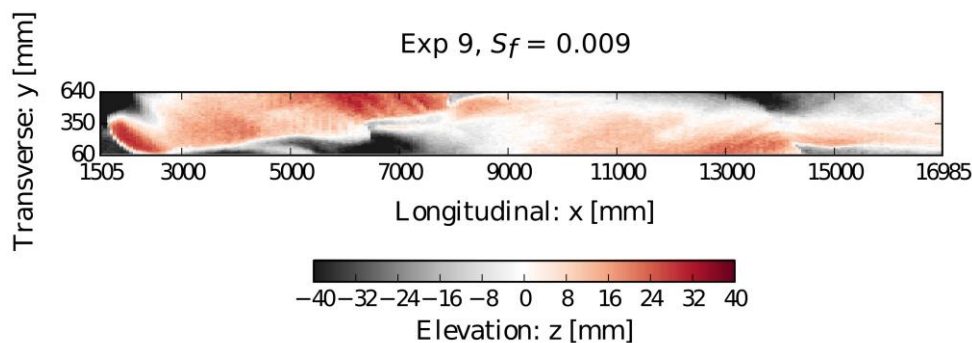


Figure 3. Detrended bed topography recorded at the end of REF.

3.2 Unsteady discharge experiments

The average bed slope and water surface slope did not change significantly during the first unsteady experiment (UF1) due to the constant coarse sediment supply rate maintained throughout the experiment (see Figure 4). We observed under the rising discharge that the pools were getting filled, and the crest of the bars did erode a bit, resulting in the increase of the bed slope near the right side (S_b [right]) of the flume and decrease of the bed slope near the left side (S_b [left]) of the flume. As the experiment progressed and water discharge decreased again, the forced bars developed further, and the pools became deeper. The slope of the bed near the left side of the flume increased due to redevelopment of the forced bars, and the slope of the bed near the right side decreased due to the deepening of the pools. Eventually, the slopes went back to their initial values.

During the second unsteady experiment (UF2), the bed slope and water surface slope decreased significantly all along the experiment, on both sides of the flume, due to sediment supply termination, as shown in Figure 4.

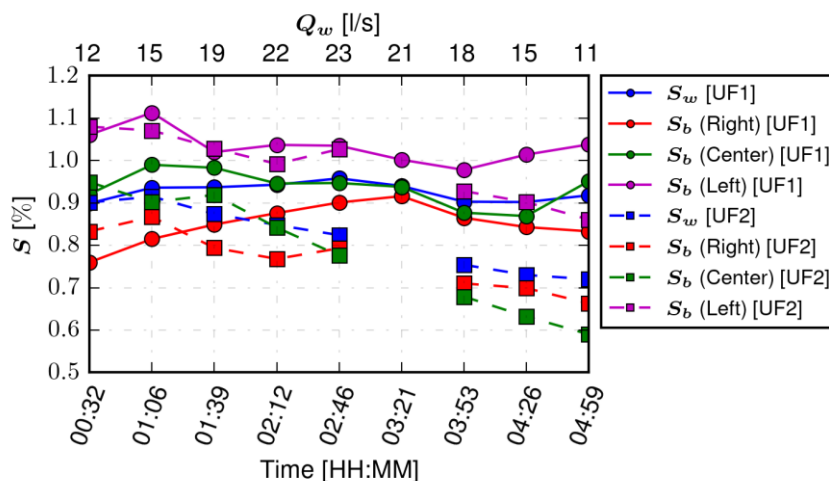


Figure 4. Evolution of the water surface slope (S_w) and bed slope (S_b) during experiments UF1 and UF2.

Figure 5 shows the longitudinal bed profiles and the difference between the left and right-side bed elevations (Δz) measured during the start, peak, and end of the experiments UF1 and UF2. No significant differences in the bed topography were observed during the first 30 minutes. When the water discharge approached its peak, the first forced bar became flatter and shorter, and the second forced bar disappeared. Free alternate bars were observed, and the bed was nearly flat from the mid to the end of the flume in the experiments UF1 and UF2, respectively. The two forced alternate bars redeveloped with different wavelengths and heights at the end of the unsteady discharge experiments.

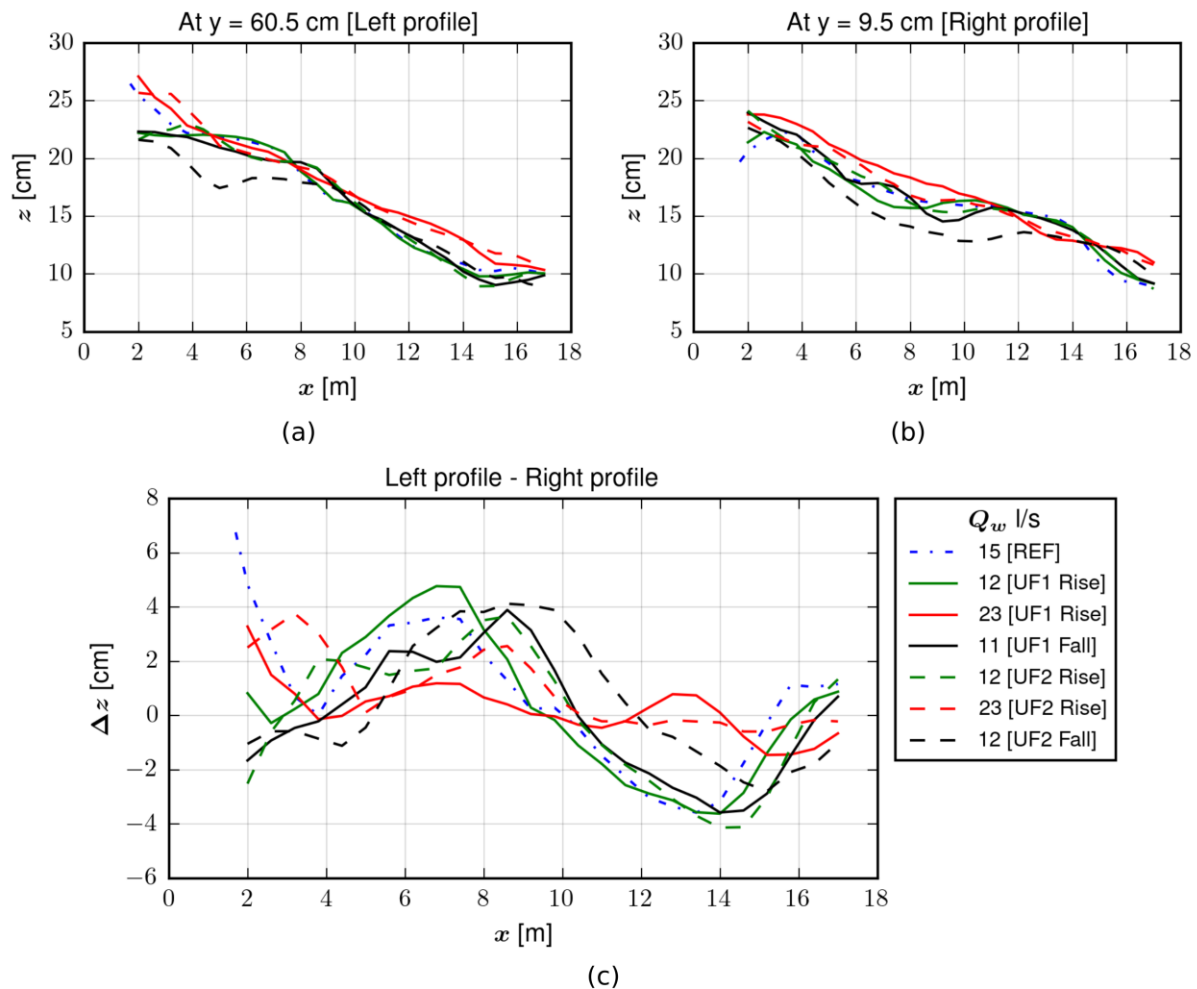


Figure 5. Longitudinal bed profiles and difference between the left and right-side bed elevations (Δz) measured during the experiments UF1 and UF2. A similar profile for the REF is plotted for comparison.

Figure 6 presents the initial and final bed topographies for the two unsteady discharge experiments. The initial bed topography for experiment UF1 is at the end of the REF experiment. The initial topography for experiment UF2 is the same as the topography at the end of UF1. The three topographies present two forced alternate bars, the first forced bar opposite the upstream forcing.

After the first unsteady flow experiment, the average slope of the bed did not change, but the wavelength of the forced alternate bars increased by 1.2 meters compared to the REF case (see Figure 6). This result was consistent with Rolin (2021) numerical results in which he noticed the elongation of the wavelength of the forced alternate bars after flood events. A major increment was observed in the length of the first forced bar. The bar height increased by 1 cm, and the bar relief did not change. Table 2 summarises the geometric characteristics of the forced alternate bars developed at the end of the three experiments.

After the second unsteady flow experiment in which the sediment supply was terminated, global erosion of the bed was recorded. The final slope of the bed decreased, and the length of the scour zone increased near the brick (see Figure 6). Two forced alternate bars were observed, shifted downstream, with the wavelength of the forced alternate bars comparable to the REF case. The height and relief of the forced bars were reduced due to the global erosion of the bed (Table 2).

Table 2. Geometric characteristics of the forced alternate gravel bars developed in the REF case and after the two unsteady discharge experiments.

| Case | Wavelength: λ_b [m] | Height: H_b [cm] | Relief: R_b [cm] | Length of first forced bar: L_1 [m] | Length of first forced bar: L_2 [m] |
|------|--------------------------------|-----------------------|-----------------------|--|--|
| REF | 12.52 | 9.6 | 1.6 | 6.42 | 6.1 |
| UF1 | 13.71 | 10.5 | 1.7 | 7.36 | 6.35 |
| UF2 | 12.3 | 8.5 | 1.2 | 6.38 | 5.92 |

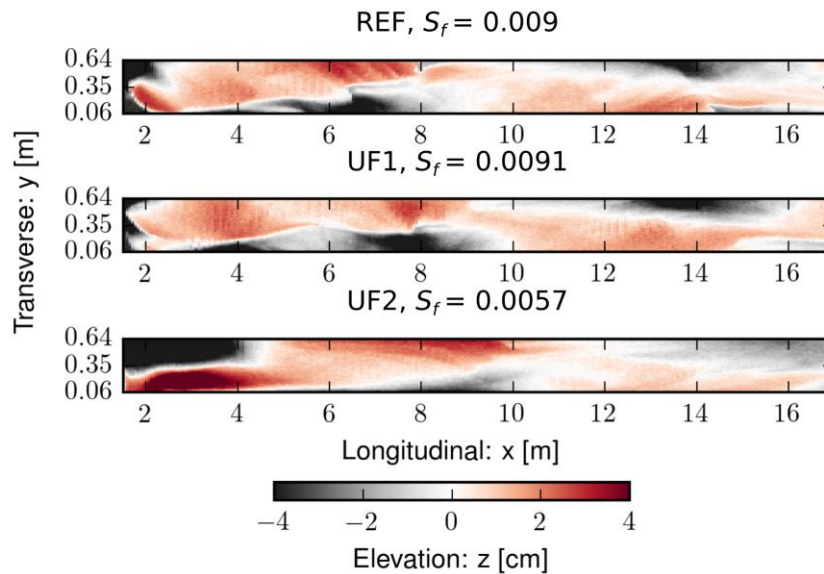


Figure 6. Detrended bed topographies recorded at the end of the three cases. The first subplot is identical to Figure 3. The title of each subplot recalls the name of the corresponding experiment and the final slope of the bed.

3.3 Comparison with the linear model of Lanzoni (2000)

We noticed substantial uncertainties in measuring the wavelengths and proxy heights of the alternate bars during unsteady discharge experiments. The uncertainties arise due to the poor spatial resolution of the bed profiles measurement and the long duration to measure the bed profiles. The time scale at which the bed was changing was shorter than the duration to measure the bed profiles. During experiment UF2, the bed slope decreased continuously, making the bed profile measurement even more uncertain. Therefore, we presented and discussed the results of the experiment UF1 only.

The evolution of the experimental wavelength and proxy height of the alternate bars observed in UF1 is presented in Figure 7, along with the experimental damping coefficient. With the linear theory of Lanzoni (2000), we computed the theoretical damping coefficient and wavelengths of the forced alternate bars, which are presented in Figure 7 (b) and (c). We identified the resonant water discharge as 18 l/s, at which the damping coefficient was zero. There should be no damping of the height of the alternate bars below 18 l/s, and the damping should be noticed after 18 l/s. We observed a decreasing trend in the height of the forced alternate bars and an increase in the damping coefficient during the rising limb of UF1. This trend was sharper as the water discharge past the resonant water discharge. The opposite trend was observed during the falling limb, leading back to values similar to the initial ones, as shown in Figure 7 (a) and (b).

The theoretical wavelength was not computed for water discharges corresponding to bed shear stress lower than the critical shear stress. It increases asymptotically when water discharge decreases toward this critical value. A minimum value for the wavelength was obtained around 19 L/s. For larger discharges, the wavelength increases with discharge. The experimental values well comply with theoretical findings. Exceptions lie in low water discharges, where the observed wavelength results from the REF experiment. Similarly, at high discharges, the wavelength at low discharges is significantly different (shorter) than what predicts theory. For these discharges, the height of the forced bars is shallow (a few centimeters), and shorter free bars emerge.

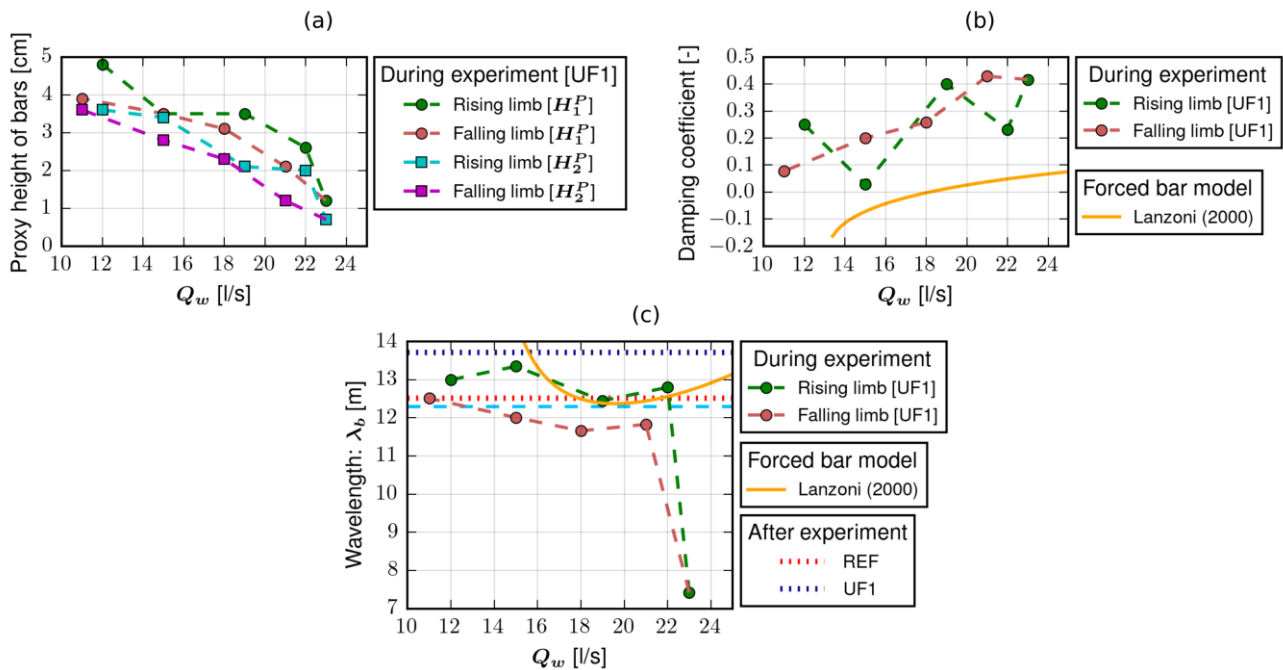


Figure 7. Evolution of the (a) proxy heights, (b) damping coefficient, and (c) wavelength of the forced alternate bars during unsteady experiment UF1.

4. CONCLUSIONS

We investigated the dynamics of two forced alternate bars under unsteady flow with and without sediment supply for a short flood event. When the flood event averaged sediment transport rate was supplied during the experiment, the sediment supply rate was good enough to maintain the average bed slope nearly constant. The first forced bar was damped in the first half of the flume, and free bars were observed in the second half of the flume at the peak of the flood. The two forced bars reemerged during the falling limb of the hydrograph and eventually redeveloped by the end of the flood event with larger wavelengths. The flow unsteadiness did not affect the dynamics of the forced alternate bars as the observed wavelengths of the bars during the experiment matched with the theoretical values of the wavelength of the forced bars computed for steady discharges.

We also demonstrated that the linear theory of Lanzoni (2000) or similar models could be used to compute the wavelengths of the forced alternate providing a suitable choice for the bedload transport formula, and friction coefficient of the bed is made. The damping coefficients from the linear theory could also be used for qualitative assessment of the behavior of the height of the forced bars under a flood event.

When the sediment supply was terminated during the flood event, the bed slope decreased throughout the experiment due to global erosion of the bed. The first forced bar was damped, and a flat bed was observed after the first bar at the peak of the flood. The forced bars reemerged and started to develop when the flood passed its peak. The two forced bars were observed at the end of the flood event with significant downstream movement. The bar height and relief of the final forced bars decreased under starving conditions, but the wavelength was close to our reference case of two forced alternate bars.

5. ACKNOWLEDGEMENTS

The research work was supported by INRAE and the French National Research Agency (ANR) under the grant ANR-18-CE01-0019-01 (DEAR project). Precious technical support of Adrien Bonnefoy and Fabien Thollet is acknowledged.

6. REFERENCES

- Colombini, M., Seminara, G., and Tubino, M. (1987). Finite-amplitude alternate bars. *Journal of Fluid Mechanics*. 181, 213-232.
- Ikeda, S. (1984). Prediction of alternate bar wavelength and height. *Journal of Hydraulic Engineering*. 110 (4), 371-386.

- Keulegan, G.H. (1938). Laws of turbulent flow in open channels. *Journal of Research of National Bureau of Standards*. 21(6).
- Lanzoni, S. (2000). Experiments on bar formation in a straight flume: 1. Uniform sediment. *Water Resources Research*, 36, 3337-3349.
- Redolfi, M., Welber, M., Carlin, M., Tubino, M., and Bertoldi, W. (2020). Morphometric properties of alternate bars and water discharge: a laboratory investigation. *Earth Surface Dynamics*. 8, 789-808.
- Roline, M. (2021). Numerical study on the development of alternate bars in varying discharge conditions. *Master thesis, Delft University of Technology*.
- Struiksma, N. and Crosato, A. (1989). Analysis of a 2-D bed topography model of rivers. *In River Meandering (eds S. Ikeda and G. Parker)*. Chapter 6.
- Talmon, A., Struiksma, N., and Van Mierlo, M.C.L.M. (1995). Laboratory experiments of the direction of sediment transport on transport alluvial-bed slopes. *Journal of Hydraulic Research*. 33, 495-517.
- Tubino, M. (1991). Growth of alternate bars in unsteady flow. *Water Resources Research*. 27, 37-52.